AFRL-RX-WP-TP-2011-4301

STRESS CORROSION CRACKING FACET CRYSTALLOGRAPHY OF Ti-8Al-1Mo-1V (Preprint)

A.L. Pilchak

Processing Section
Metals Branch

A.H. Young and J.C. Williams

The Ohio State University

MAY 2011

AIR FORCE RESEARCH LABORATORY
MATERIALS AND MANUFACTURING DIRECTORATE
WRIGHT-PATTERSON AIR FORCE BASE, OH 45433-7750
AIR FORCE MATERIEL COMMAND
UNITED STATES AIR FORCE

REPORT DOCUMENTATION PAGE

Form Approved
OMB No. 0704-0188

1. REPORT DATE *(DD-MM-YY)*	2. REPORT TYPE	3. DATES COVERED *(From - To)*
May 2011	Journal Article Preprint	01 May 2011 – 01 May 2011

4. TITLE AND SUBTITLE
STRESS CORROSION CRACKING FACET CRYSTALLOGRAPHY OF Ti-8Al-1Mo-1V (Preprint)

5a. CONTRACT NUMBER
In-House

5b. GRANT NUMBER

5c. PROGRAM ELEMENT NUMBER
62102F

6. AUTHOR(S)
A.L. Pilchak (Metals Branch, Processing Section (AFRL/RXLMP))
A.H. Young and J.C. Williams (The Ohio State University)

5d. PROJECT NUMBER
4347

5e. TASK NUMBER
20

5f. WORK UNIT NUMBER
25100102

7. PERFORMING ORGANIZATION NAME(S) AND ADDRESS(ES)

Metals Branch, Processing Section (AFRL/RXLMP)
Materials and Manufacturing Directorate, Metals, Ceramics, and NDE Division
Air Force Research Laboratory
Wright-Patterson Air Force Base, OH 45433-7750
Air Force Materiel Command, United States Air Force

The Ohio State University

8. PERFORMING ORGANIZATION REPORT NUMBER
AFRL-RX-WP-TP-2011-4301

9. SPONSORING/MONITORING AGENCY NAME(S) AND ADDRESS(ES)

Air Force Research Laboratory
Materials and Manufacturing Directorate
Wright-Patterson Air Force Base, OH 45433-7750
Air Force Materiel Command
United States Air Force

10. SPONSORING/MONITORING AGENCY ACRONYM(S)
AFRL/RXLM

11. SPONSORING/MONITORING AGENCY REPORT NUMBER(S)
AFRL-RX-WP-TP-2011-4301

12. DISTRIBUTION/AVAILABILITY STATEMENT
Approved for public release; distribution unlimited.

13. SUPPLEMENTARY NOTES
PAO case number 88ABW-2010-3856, cleared 16 July 2010. The U.S. Government is joint author of this work and has the right to use, modify, reproduce, release, perform, display, or disclose the work. Submitted to Corrosion Science. Document contains color.

14. ABSTRACT
The spatial and crystallographic orientations of facets formed during stress corrosion cracking of Ti-8Al-1Mo-1V have been characterized using quantitative fractography and electron backscatter diffraction. The results indicate that most facets are formed nearly perpendicular to the loading direction on irrational {hkil} planes. The facets were imaged with high resolution scanning electron microscopy and were found to contain evidence of localized plastic flow despite their "brittle" appearance at moderate magnification. Some fracture planes were related to titanium-hydride habit planes; however, the mechanism of faceted growth does not appear to involve hydride nucleation, growth, and fracture, but rather hydrogen enhanced localized plasticity.

15. SUBJECT TERMS
stress corrosion cracking, titanium, SEM, hydrogen embrittlement

16. SECURITY CLASSIFICATION OF:			17. LIMITATION OF ABSTRACT:	18. NUMBER OF PAGES	19a. NAME OF RESPONSIBLE PERSON (Monitor)
a. REPORT	b. ABSTRACT	c. THIS PAGE			Donna Ballard
Unclassified	Unclassified	Unclassified	SAR	40	19b. TELEPHONE NUMBER *(Include Area Code)* N/A

Stress corrosion cracking facet crystallography of Ti-8Al-1Mo-1V

A.L. Pilchak[a,b,*], A.H. Young[c] and J.C. Williams[c]

[a]Air Force Research Laboratory, Materials and Manufacturing Directorate, RXLMP, Wright Patterson Air Force Base, OH 45433

[b]Universal Technology Corporation, Dayton, OH 45432

[c]The Ohio State University, Department of Materials Science and Engineering, Columbus, OH 43210

*Corresponding author:

Adam L. Pilchak, PhD

Air Force Research Laboratory

Materials and Manufacturing Directorate

2230 Tenth St.

Bldg 655 Rm 126

Wright Patterson Air Force Base, OH 45433

email: adam.pilchak@wpafb.af.mil

phone: +1-937-904-5992

Abstract

The spatial and crystallographic orientations of facets formed during stress corrosion cracking of Ti-8Al-1Mo-1V have been characterized using quantitative fractography and electron backscatter diffraction. The results indicate that most facets are formed nearly perpendicular to the loading direction on irrational {hkil} planes. The facets were imaged with high resolution scanning electron microscopy and were found to contain evidence of localized plastic flow despite their “brittle” appearance at moderate magnification. Some fracture planes were related to titanium-hydride habit planes, however, the mechanism of faceted growth does not appear to involve hydride nucleation, growth, and fracture, but rather hydrogen enhanced localized plasticity.

Key words: C. stress corrosion cracking; A. titanium; B. SEM; C. hydrogen embrittlement

Introduction

Stress corrosion cracking (SCC) of titanium alloys is a phenomenon that occurs due to the combined effects of an externally applied stress and a corrosive environment in the presence of a sharp notch or crack [1]. The requirement for a notch, or similar stress concentration, to initiate SCC in titanium alloys makes them unique compared to other alloy systems. In general, the environment acts to accelerate the growing crack leading to premature failure compared to cracks growing in air. Titanium is naturally passive at room temperature in neutral aqueous solution, even those containing chlorine (Cl^-) ions, due to the presence of a highly adherent, protective TiO_2 film that forms spontaneously on its surfaces [2]. Titanium remains passive, in accordance with the Pourbaix diagram, as long as the film is present. However, the film can be ruptured during mechanical loading, or if it comes in contact with an abrasive media, which permits direct interaction between titanium and the environment resulting in SCC.

A number of corrosive environments, like nitric acid, various molten salts, nitrogen-tetroxide, several organic solvents and methanol are known to cause SCC of titanium alloys [3]. It is noteworthy, however, that SCC is most prevalent in less harsh environments which do not tend to excessively corrode and blunt the crack tip. As a result, SCC occurs readily in an aqueous 3.5 pct. NaCl solution making this vulnerability a practically important issue since many titanium alloy components encounter such an environment in service. Since it is conceivable that the passive film could be ruptured on any component, whether due to mechanical loading, foreign object damage, or otherwise, it is necessary to understand the mechanisms by which stress corrosion cracks can form at the free surfaces of specimens, and, perhaps more importantly, how these cracks subsequently propagate faster than those growing in air.

The effects of composition and microstructure on the susceptibility of titanium alloys to SCC can be difficult to separate [3]. All classes of titanium alloys, α, α + β and β alloys, have been demonstrated to be

susceptible to SCC [4] under the right circumstances, with the composition of each constituent phase having the strongest influence on the relative degree of susceptibility [3]. In near-α alloys, like the Ti-8Al-1Mo-1V (Ti-811) alloy investigated in this work, the composition of the α phase, and in particular, aluminum (Al) and oxygen (O) content, plays an important role in the SCC behavior. Blackburn and Williams [5] have observed a correlation between the increased susceptibility to SCC and the increased propensity for planar slip due to Al and O additions [3;7]. At higher Al concentrations, with an appropriate aging treatment, the ordered α_2 phase (Ti_3Al) can be precipitated within the α phase in the form of fine, coherent particles that are only directly observable with transmission electron microscopy. Because this phase is coherent with the α phase matrix, it can be sheared by moving dislocations. In accordance with classical theory, once particles are sheared on one slip band, it becomes increasingly easier for subsequent dislocation motion on that plane. This is particularly true for the hexagonal close packed (HCP) α phase because activation of other slip systems is less likely because they almost always have a low Schmid factor compared to the operative one. Thus, although the particles slightly increase the strength of the alloy, they also have the effect of further localizing slip and decreasing ductility. With regard to SCC, the α_2 phase has several important implications. Blackburn and Williams [5] have shown that the presence of α_2 decreases the critical stress intensity required to initiate SCC and subsequently increases crack tip velocity by approximately four times in Ti-811 compared to the non-α_2 containing condition. Based on empirical evidence, α_2 also appears to affect the electrochemical reaction occurring at the crack tip, however, the operative physical mechanism remains elusive. Although there is no quantitative treatment available, it is known that O acts as an α_2 stabilizer and allows for the $\alpha + \alpha_2$ phase field to exist at higher temperatures [2].

Observations of specimens that have failed by SCC generally reveal regions of flat, faceted features on the fracture surface consistent with transgranular fracture of the α phase, although other features like dimples

and ductile tear ridges also are almost always present in some localized area on the fracture surface [3]. The latter features are most commonly associated with fracture of the transformed β regions consisting of fine acicular α (or α') [5]. The facets have been called cleavage facets [5;8-10] or cleavage-like facets [3], although it is important to recognize that this terminology is based solely on appearance of these features and it has not yet been shown that cleavage, at least in the classical sense [11], was operative.

The correlation between slip behavior and SCC susceptibility, combined with the observations of planar, faceted features on fracture surfaces, has been used by some authors to advocate a slip-based mechanism to explain SCC. For example, Zhang and Vereecken [12] have proposed a mechanism for stress corrosion cracking in Ti-6Al-4V with a coarse lamellar microstructure where slip planes oblique to the loading direction cause mechanical rupture of the protective oxide film which allowed hydrogen in the environment to penetrate the specimen. The authors suggested that the movement of dislocations increased the "reactivity of atoms along the dislocation lines" that resulted in preferential dissolution of atoms along the slip band resulting in the formation of a narrow crack along the slip band. They suggested that fracture of material between parallel inclined cracks was responsible for forming facets perpendicular to the loading direction. While slip traces were observed on the surfaces of the specimens, there was no evidence provided that confirmed that fracture indeed occurred along these slip bands.

Gregory and Brokmeier [9] have reported on the effect of microstructure and texture on SCC susceptibility in Ti-6Al-4V in 3.5 pct. NaCl. The results showed that the relative SCC sensitivity K_{ISCC} / K_{IQ} correlated well with the relative intensity of basal poles parallel to the tensile axis. The authors interpreted this as evidence of brittle fracture and not slip on basal planes as being responsible for the increased cracking rates. Based solely on the orientation dependence of K_{ISCC}, the authors argued in favor of a mechanism involving brittle fracture of hydrides. However, while it is possible to infer fracture mechanisms based on macroscopic

material response, the micromechanisms of crack growth can best be understood using direct observation in the electron microscope.

Based on crack growth experiments conducted in hydrogen gas, the effect of hydrogen on fracture topography is manifested as localized tear ridges and dimples [13-15], but the embrittling effects are only realized through macroscopic stress-strain response [15]. High resolution electron microscopy studies [14] of such specimens have revealed features consistent with fractured hydrides directly on the fracture surface (Figure 1) that have plate-like morphology and dimensions consistent with hydrides that have been observed in the transmission electron microscope [16;17]. These features were situated in shallow dimples surrounded by tear ridges suggesting there was localized plastic deformation at the hydride / matrix interfaces. Relatively few fractured hydrides were observed, however, and the majority of the facets were covered with tear ridges. There were two length scales of tear ridges, those we call “primary ridges” designated by the letter B in Figure 1 and a series of smaller, both in length and height, “secondary ridges” identified by letter C. In contrast, most studies of SCC in titanium alloys report finding “cleavage” facets [8-10] on the fracture surface and do not provide evidence for plasticity. Ridges, as depicted in Figure 1, are different than steps, which are commonly observed on titanium alloy facets formed during cyclic loading in air [18]. The latter are sharp, angular features which are complementary on mating fracture surfaces whereas the ridges match point-to-point [11;19].

Shih et al. [16] have studied the mechanisms by which hydrogen interacts with growing cracks in binary Ti-4Al by deforming samples *in situ* in a transmission electron microscope equipped with an environmental cell. Two hydrogen-assisted crack advance mechanisms were observed. The first, which was dominant at low crack growth rates, was stress-assisted hydride nucleation, growth and subsequent crack extension by fracture of the hydrides. This mechanism corresponded with slow crack growth rates due to the sluggish

kinetics of hydride formation. It took approximately ~14 minutes for the first hydride to form at a pressure of 16 kPa while the coarsening rates were observed to be ~ 3 nm s^{-1}. It might be expected that this mechanism would be even slower when a reservoir of gaseous hydrogen is not available. In the second mechanism, operative at high crack growth rates where repeated hydride formation and fracture is not possible, hydrogen acted to locally reduce the stress required for dislocation motion as well as to increase the velocity of dislocations [15;16]. The result is highly localized slip in the vicinity of the crack tip, which was observed to start and stop as hydrogen was added and removed from the environmental cell, respectively [16]. Since the concentration of hydrogen is increases with higher local elastic strains, it was greatest at the singularity created at the crack tip and thus the fracture processes were highly localized and constrained to this region. With regard to macroscopic material behavior, since these processes occurred below the macroscopic yield strength, the net response of the material would appear to be brittle. Although the alloy studied by Shih et al. [16] was binary Ti-4Al, similar behavior would be expected in the α phase in the present alloy, although the higher Al concentration would affect the solubility of hydrogen in the α phase [20] and also alter the slip character / critical resolved shear stresses of the various slip systems [7]. In addition, alloys with high Al content are more prone to the formation of α_2 which, as mentioned above, have been empirically determined to be more sensitive to SCC [20;21].

Moody and Costa [20] have suggested the increased susceptibility is related to the high degree of slip localization observed in alloys containing α_2 [7]. They argue that as slip planarity increases, the strain within each slip band increases and so they are able to more easily nucleate hydrides. The authors showed many examples of the correlation between composition and stress corrosion cracking susceptibility that coincided with increased tendency for slip planarity, but there was no experimental evidence provided that hydrides were formed or fractured. In contrast, Curtis, Boyer and Williams [4] have argued that slip localization due to the presence of α_2 has the effect of restricting crack tip blunting. The consequence of this is that a

sharper crack tip is maintained resulting in a larger stress concentration at the crack tip. Thus, the driving force for continued crack extension remains high rather than periodically strengthening / weakening, as one might expect for a situation where the crack tip is repeatedly blunted / resharpened.

If the operative fracture process during SCC was related to formation of hydrides on planar slip bands and subsequent fracture of these hydrides [20], or due to preferential dissolution of atoms along a slip band [12], it would logically be expected that the fracture plane would coincide with the slip band on which the hydride precipitated. For example, the fracture plane of small fatigue cracks in titanium alloys growing under constant cyclic stress amplitude have been shown to correspond precisely with the active slip plane along which they are growing in Ti-6Al-4V [18;23] and Ti-811 [24]. In contrast, the crystallographic plane of fracture during SCC is frequently reported to be between 10^o and 15^o from the (0001) plane [3;5;8]. Due to earlier limitations in experimental capability, these facet planes were primarily determined by Laue x-ray measurements made on coarse grained material. The results of these early studies are briefly summarized below.

Blackburn and Williams [5] have summarized the fracture planes for SCC of various near-α titanium alloys in water, air, NaCl solution, methane, carbon tetrachloride and hexane. In all instances, the facet plane was between 12^o and 16^o from the basal plane, except for one instance of Ti-811 fractured in hexane where the facet plane was approximately 6^o from (0001). Of the reported data, the most preferred fracture plane was 15^o from (0001), close to the $\{10\bar{1}7\}$ plane. Meyn [8] examined the effect of frequency and microstructure on cyclic stress corrosion cracking in Ti-811. In the study, Meyn observed facets on fracture surfaces created at low (0.5 Hz) and high (30 Hz) test frequencies, and by static loading, and determined that they were either parallel to (0001) or were approximately 15^o from (0001)α, also near $\{10\bar{1}7\}$, which was

consistent with earlier reports [3;5]. Meyn recognized that these fracture planes, and the features on the facets, were similar to those formed by sustained load cracking in H_2 gas [25] implying there was a similar mechanism operative in both cases. Interestingly, both the basal plane and the near-$\{10\bar{1}7\}$ irrational fracture planes corresponded well with known hydride habit planes [26]. Although it is tempting to relate the fracture mechanism to hydride nucleation, growth and fracture, there remains no direct experimental evidence that such a phenomenon is occurring. Thus, the mechanism of crack growth during SCC remained an open question for several decades.

Since the initial studies summarized above have been performed, there have been significant advances in the resolution of scanning electron microscopes and, furthermore, more precise methods to determine the spatial and crystallographic nature of facet planes have become available [27-29]. Thus, in the present study, the fracture surface topography along with the spatial and crystallographic orientations of stress corrosion cracked specimens of Ti-8Al-1Mo-1V are analyzed by coupling high resolution scanning electron microscopy and electron backscatter diffraction (EBSD) techniques. The use of EBSD and quantitative tilt fractography [27;29] allow for determination of the crystallographic fracture plane to an accuracy between 1^o [29] and 3^o [30] without *a priori* knowledge of the spatial orientation of the fracture plane. The method has been described in detail in the literature [27-29], but briefly, it involves finding the spatial orientation of the facet within the same sample reference frame used for EBSD analysis and connecting the two reference frames using inverse pole figures (IPF). Using this method, both the spatial orientation of the facet with respect to the loading direction as well as the crystallographic plane of fracture is determined, both of which aid in assessing the possible micromechanisms of crack growth. This method serves as a higher fidelity check of the measurements made much earlier using x-ray techniques on coarse grained

materials [3;8]. Since the interaction volume associated with EBSD is very small, this method can be applied precisely to individual facets on fine-grained material in production form [23;28;29].

Materials and methods

Ti-8Al-1Mo-1V bar, with a diameter of 12.7 cm and length of approximately 127 cm, was provided by Timet (Henderson, NV). Metallographic sections were prepared parallel and transverse to the bar axis by rough grinding with progressively finer SiC papers through 600 grit followed by polishing with diamond compounds of 9 μm, 6 μm, 3 μm, and 1 μm. Final polishing was performed overnight on a vibratory polisher containing 0.05 μm non-crystallizing colloidal silica. The microstructures were investigated using a field emission source scanning electron microscope (SEM) that also had a commercially available EBSD system which was used to assess the degree of preferred orientation in the material. EBSD analysis was performed over large areas on longitudinal sections cut along the bar axis so that the area analyzed would be representative of a cross section of the specimen gauge sections. The EBSD experiments were conducted at an accelerating voltage of 20 kV and a beam current of approximately 10.5 nA. Such high probe current was achieved using a 100 μm diameter aperture and was found to be beneficial for generating high quality EBSD patterns. Several scans were taken at various depths along the bar axis during the preparation of specimens for this and other studies utilizing the same material [24]. The microstructure and texture was remarkably similar at all locations investigated. The representative scan presented in this study was 4.12 mm x 2.91 mm acquired at a step size of 5 μm using a combination of beam scans and automated stage movements.

Tensile specimen blanks were excised transverse to the bar axis via wire electric discharge machining (EDM). One blank was wrapped in tantalum foil and heat treated for 24 hours at 525 ^{o}C in argon atmosphere to precipitate α_2 particles. The blanks were then machined into round tensile specimens that

were 57.15 mm long, with a gauge length of 15.88 mm and diameter of 4.06 mm (surface finish: longitudinal polish, 0.8 μm average roughness). Specimens in the as-received and aged conditions were statically loaded in an aqueous 3.5 pct. NaCl solution using an M-Cert Test System (InterCorr International, Inc., Houston, TX). The system utilizes a high precision step-motor to change displacement in order to maintain a constant stress in the gauge section of the sample. The specimens were ramped to a constant stress of 758 MPa at a rate of 10^{-2} mm/s, which is 95 pct. of the 0.2 pct. offset yield strength of the as-received condition, and held until failure. Due to the slight precipitation hardening effect of α_2, this level of stress was less than 95 pct. of the yield strength for the aged specimen, however, the actual yield stress of this condition was not determined. As mentioned above, Ti-8Al-1Mo-1V exhibits increased susceptibility to stress corrosion cracking in the presence of a notch. Thus, since the purpose of this study was to create facets for analysis, four 0.5 mm to 1 mm diamond scribe lines were made around the circumference of the specimen at varying positions along the gauge length of the specimen.

Upon completion of the test, the as-fractured specimens were protected with Miccrostop (Tolber Chemical Division, Hope, AK), an acrylic lacquer and sectioned transverse to the loading direction via wire electrical discharge machining. After sectioning, the specimens were ultrasonically cleaned in acetone to remove the Miccrostop, then cleaned with distilled water and finally with isopropyl alcohol followed by drying with compressed air. The specimens were mounted to a stub with colloidal graphite and examined in the SEM. Fractographic analysis was performed in an FEI Sirion (FEI Company, Hillsboro, OR) equipped with a field emission source. The Sirion SEM has an ultra-high resolution (UHR) mode in which a scintillator-type detector located in the pole piece is used to collect only the highest energy electrons. The detector can be negatively biased to collect backscattered or positively biased to collect secondary electrons. A bias of +20V was utilized for the present study.

Results

Microstructure

The microstructure of the as-received material, shown in Figure 2, consisted of 20 μm globular α grains and packets of α + β colonies that were between 10 μm and 20 μm. The volume fraction of globular α was on the order of 60 pct. A representative EBSD scan and the associated pole figures are shown in Figure 3 and Figure 4, respectively. The pole figures show a peak intensity of only 1.8x random indicating that macroscopically, the material is not strongly textured. However, it is evident from the crystal orientation map in Figure 3 that there are bands of similarly oriented grains running across the gauge section of the specimens. These are known in the titanium literature as microtextured regions [31] (or 'macrozones'), and are a consequence of heterogeneous deformation during thermomechanical processing arising from the plastic anisotropy of the α phase [Bieler 2002]. The pole figures indicate that there was not a significant variation in the density of basal poles oriented between 0^o and 90^o from the loading direction. This is important because it means that the crystallographic orientations of the grains in which the cracks initiated were not biased by macroscopic texture effects. Even the slight variations between 1.5x and 1.8x random would be eliminated if we imposed sample symmetry consistent with the axisymmetric deformation path used to thermomechanically process the bar, which might be expected to be more representative of the texture through the thickness as opposed to the two-dimensionsal section analyzed here. It is also noted that the heat treatment temperature and time were too low and too short, respectively, to cause any change in microstructure at the constituent level. However, the macroscopic behavior of the sample, as described subsequently, confirmed that Ti_3Al was indeed precipitated within the α phase.

Test results

Since the purpose of this study was to create facets for electron microscopy analysis, no extensive data acquisition was performed during testing, however the time to failures of the specimens illustrate an

important difference. The as-received specimen failed after 10 hours 31 minutes whereas the specimen in the aged condition failed in 1 minute 31 seconds implying that the crack incubation time was reduced and the crack growth rate was significantly increased by the presence of α_2, consistent with previous work [5].

Initial assessment of the fracture surfaces

Secondary electron images of the transverse cross sections of the fractured specimens are shown in Figure 5. The fracture surfaces were considerably different depending on the microstructural condition. In the as-received condition, multiple cracks grew inward both from the scribe lines as well as from surface imperfections and eventually the ligaments between these cracks fractured to form the rough surface topography evident in Figure 5. In contrast, the fracture surface of the aged specimen was macroscopically more flat with one large faceted region spanning the entire diameter of the gauge section. Two other millimeter sized faceted regions were also observed to penetrate part of the way through the gauge section. In both specimens, the regions not characterized by faceted fracture generally consisted of features like flutes [33;34] and dimples consistent with ductile fracture. Shear lips were present at the location of final fast fracture on both specimens. The size and shape of the faceted regions is consistent with the length scale of the microtextured regions evident in Figure 3.

There were no faceted regions that directly bordered the surface of the as-received specimen, however, the facets designated by ‘a’ in Figure 5 were approximately 25 μm from the surface and the markings on the facets indicated the crack was growing toward the specimen interior. Thus, it could be inferred these facets formed at a small crack length. Those facets at location ‘b’ (near the opposite edge of the sample) are considered to be propagation facets because the markings on the facet indicated the crack was growing towards the sample surface. In contrast, there were facets that bordered the surface of the sample on both sides of the gauge section of the aged specimen. The facet markings indicated that these were both crack

entry locations which propagated and met in the middle of the specimen around location 'b'. These cracks did not enter the specimen at the scribe lines but rather at the smaller imperfections left on the surface of the specimen by the machine tooling, or at notches created by plastic-deformation-induced surface roughening. These observations suggest that α_2 significantly enhances SCC notch sensitivity in Ti-811. In the next section, the facets at each of these locations are discussed in more detail.

High resolution fractography

As-received specimen

Higher magnification images of the initiation and propagation facets on the as-received specimen that were studied in detail here are shown in Figure 6. The three facets in this near surface region that were studied in detail have been designated H3-1-1, H3-1-2 and H3-1-3 in Figure 6. The lowest magnification of this region is shown in Figure 6(a), where the specimen surface is evident as the out of focus region in the lower right corner of the image. Between the facets and the surface was a region of dimpled fracture and serpentine glide. The latter features resemble fatigue striations and are more evident in the lower right corner of Figure 6(b). However, no cyclic load was applied and thus these features are actually formed by the intersection of slip bands with the fracture surface, often called serpentine glide [35]. Slip bands were also evident on several of the facet surfaces, however they were considerably more planar than those observed in the regions of serpentine glide. Facet H3-1-2 is shown at high magnification in Figure 6(c). A series of small, parallel ridges were evident on the facet surfaces that extend in the direction of crack growth (feature 1). There were also planar slip bands evident with spacing of 500 nm to 1 μm (feature 2) that were apparent on the facet surfaces. These slip bands were transverse to the ridges and, therefore, to the local crack propagation direction.

Several propagation facets located on the other side of the specimen from those facets discussed above are shown in Figure 6(d). Two of these facets, H3-1-4 and H3-1-5, were investigated in detail and are shown at higher magnification in (e) and (f). Facet H3-1-4 contained both steps, which formed terraces of varying height, as well as primary and secondary tear ridges on each of the individual terraces indicating localized plastic flow on the terrace planes. In contrast, facet H3-1-5 appeared much more similar to those facets observed at small crack lengths with only fine secondary ridges present and generally fewer features than facet H3-1-4. No slip traces were observed on either of these facets. Upon closer inspection (Figure 6(f)) it is evident that the ridges interact in a number of different ways with the grain boundary, and also with one another. For instance, one ridge turns sharply when it encounters the grain boundary and travels parallel to the grain boundary before turning sharply again and entering facet H3-1-4. Some ridges coalesce to form one, others become more intense after crossing the grain boundary and others decrease in height and eventually become indistinguishable from the facet plane.

Aged specimen

The facets on the aged specimen that was statically loaded in an aqueous 3.5 pct. NaCl solution (Figure 7) contained ridges that were similar to those observed on the specimen in the as-received condition. In general, however, the density of ridges on each individual facet was lower on the aged specimens, although the single ridges on the facets of the aged specimen were typically larger than any of the ridges on the specimen in the as-received condition.

Examination of the markings on the facets in this region (Figure 7(a) and (b)) suggested that the crack started at surface connected grains H3-2-1 and subsequently propagated into the surrounding grains (H3-2-2 through H3-2-6). While these facets appear very brittle at moderate magnifications, the evidence of plasticity becomes clear when using UHR mode at high magnification (Figure 7(d)). Some features of the

microstructure, and an indication of the relative ease of crack propagation, can be inferred from the topography of the fracture surface (Figure 7(c)). The linear boundary between facets H3-2-4 and H3-2-5, combined with the differently oriented facet planes, suggests that this is a boundary between two α grains whereas the thin strip between facets H3-2-4 and H3-2-6 has several smaller facets at various angles to one another consistent with fracture through transformed β. The two facets observed at longer crack lengths had generally rougher surfaces than those at small crack lengths (Figure 7(e)), but still had similar ridge formation and local plastic flow at high magnification (Figure 7(f)). Although the surfaces were somewhat rougher, they were still macroscopically planar and EBSD patterns could be easily obtained from them, as discussed in more detail in the next section.

Quantitative tilt fractography / EBSD analysis

All of the facets which were given identification numbers in the preceding sections were analyzed with the combined electron backscatter diffraction / tilt fractography technique [27;29] to determine both their spatial orientation with respect to the loading direction as well as their crystallographic plane of fracture. Based on the size and shape of the facets, they are all believed to have formed through globular α grains as opposed to transformed β regions. Furthermore, fracture of the β ribs in lamellar constituents is known to leave a distinctly different surface appearance during monotonic and cyclic loading [18], and it is known that the α and β phases exhibit different degrees of susceptibility to SCC [22], and so it would be expected that this trend would also hold for facets formed by SCC. The results from the orientation investigations for the as-received and aged specimens are shown on the inverse pole figures in Figure 8 and Figure 9, and also in Table 1 and Table 2, respectively. The grains analyzed in the as-received condition represent a wide range of c-axis inclinations with respect to the loading direction. For example, grain H3-1-4 has [0001] parallel to the loading direction while grains H3-1-2 and H3-1-3 have their c-axes inclined 45^{o} and 47^{o} from the loading direction, respectively, while the remaining facets were at various angles between these two extremes.

Despite this wide range of grain orientations, all of these grains fractured by facet formation on a plane between 5° and 15° from the basal plane. There was no clear correlation between deviation of the facet plane from the basal plane and the inclination of the c-axis from the loading direction. For instance, facets H3-1-2 and H3-1-5 both fractured on a plane 15° from (0001), but had their c-axes at angles of 18° and 47° from the loading direction, respectively. Facets H3-1-4 and H3-1-3 both fractured approximately 5° from (0001), yet had their c-axes parallel and at 45° relative to the loading axis, respectively. With regard to spatial orientation, the facet normal directions on the as-received specimens ranged from highly inclined at small crack lengths (facets H3-1-1 through H3-1-3) to more nearly perpendicular (facets H3-1-4 and H3-1-5) at longer crack lengths as shown in Table 1.

In contrast, the facets on the aged specimen favored orientations more nearly perpendicular to the loading direction (Table 2), despite having c-axis orientations inclined as far as 27° from the loading direction in some cases. This orientation has sufficient resolved shear stress that slip could easily occur on the basal plane, yet the crack has formed on irrational {hkil} planes oriented nearly perpendicular to the loading direction. Crystallographically, all of the fracture planes on the aged specimen were more highly inclined to the basal plane, typically between 10° and 20°, although one facet (H3-2-4) formed on a plane only 4.5° from (0001). This grain had its c-axis oriented 30° from the loading direction, the highest among all facets analyzed on this specimen, meaning it had the highest resolved shear stress on the basal plane. This may help explain why the facet formed on a different plane than the other grains, however, the change in fracture plane could not be solely attributed to crystallographic orientation because this grain was in nearly the same orientation relative to the loading axis as grain H3-2-6 which fractured approximately 20° from (0001), but on a plane nearly perpendicular to the loading direction. The relatively small deviation among

the basal poles in all grains analyzed in the aged specimen is consistent with them belonging to the same microtextured region, as suggested by the macroscopic fracture surface appearance (Figure 5).

Discussion

One of the most striking features about the fracture surfaces on the specimens is the length scales over which faceted growth is operative. In general, fracture surface morphology changes with increasing crack length due to the increase in ΔK and a concomitant increase in the cyclic crack tip plastic zone size which is related to the fracture process zone size [24;36;37]. In cyclically loaded specimens, this is manifested as faceted growth at small crack lengths, which transitions to striation growth at longer crack lengths until finally becoming unstable and rupturing by fast fracture. This final stage is generally accompanied by dimple formation. In stark contrast, the fracture mode on the as-received specimen studied here switches from ductile dimple / fluted growth [34] to faceted growth with increasing crack length. Since crack formation occurred at the surface, this point is illustrated by the non-surface-connected faceted regions in Figure 5 to the left of region 'b' and above region 'a', for example. This implies that the underlying crystallographic orientation more strongly influences fracture topography than does the size of the crack tip plastic zone relative to the microstructural constituent length scale.

As previously mentioned, the macroscopic texture of the bar was such that all the basal pole orientations relative to the loading direction were nearly equally likely. All of the grains analyzed in the aged specimen had their basal poles inclined between 20^{o} and 30^{o} from the loading direction, thus none of the grains were in exceptionally "hard" or "soft" orientations (having their c-axes parallel or perpendicular to the loading direction, respectively [38]). While no facets directly bordered the surface of the as-received specimen, facets H3-2-1 and H3-2-2 were identified as initiation facets on the aged specimen in the sense that the markings on the facets indicated that they were the grains through which the crack formed and propagated

into the surrounding microstructure. Thus, it is useful to study these facets in particular, since they represent facets favorably oriented for surface crack initiation, while the remaining facets represent propagation facets.

These grains were oriented such that slip could have easily occurred on the basal plane and, furthermore, the actual basal slip systems with the highest resolved shear stresses in each grain were oriented such that their operation could create a slip step on the surface of the specimen. However, despite these seemingly fortuitous alignments for easy slip band formation and subsequent propagation along this slip band according to conventional wisdom, the initiation facet normal directions were only 8.9^{o} and 4.3^{o} from the loading direction, respectively, indicating that the fracture plane was crystallographically irrational and inclined substantially to the basal plane (Table 2). Thus, even if slip bands were responsible for creating the stress concentration which allowed the crack to form, there was a stronger driving force for propagation along an irrational {hkil} plane as opposed to along the basal slip band. The spatial orientation of the facet normal direction can be used as an indicator of the primary force driving crack extension. The largest energy release rate per unit crack extension is achieved in mode I [39] (normal stress driven, perpendicular facets) and thus all cracks would naturally prefer to propagate in this way if there weren't other easier paths provided due to defects in the microstructure, or restriction of the crack to a particular slip plane. These latter cracks are generally driven by mode II (shear stress driven, inclined facets) forces.

The isolated cluster of facets in the as-received specimen at location 'a' (Figure 5) are a representative example of typical inclined facets. These facet planes were inclined between 29^{o} and 37^{o} to the loading direction, and furthermore, slip traces were directly observed on facet H3-1-2. It is noteworthy, however, that the slip traces were not associated with the ridges implying their formation was not related to constituent sized planar slip bands, but rather they were formed during crack extension by some other

mechanism. In order to verify this, the tilt fractography technique was used to find vectors in the plane of the facet that were parallel to the trace of the ridges or, alternatively, the crack propagation direction on individual facets. This method has been used previously [18] to correlate the steps on facets formed during continuous cycling with the slip direction of the slip system that was active during deformation indicating that the crack propagated precisely along a slip band. In contrast, a wide range of results were found for each individual facet in the present study. The data from facet H3-1-4 are used to illustrate typical results from these calculations (Figure 10). Unit vectors were determined in the plane of the facet parallel to both primary and secondary ridges, then inverse pole figures were calculated relative to these crack propagation direction, as described in [18], to determine the crystallographic direction of crack propagation. The ridge direction varied continuously and varied over an angular range of 60^{o} on the facet surface. On this particular facet, none of the ridge directions were parallel to a crystallographic slip direction, or the trace of a slip plane in the facet surface. This is in contrast to slip-band induced steps which are parallel to one another and also to a crystallographic slip direction, such as those observe in Ti-6Al-4V [18], for example. These observations further support the notion that the ridges are not associated with grain-sized slip bands, but rather form by some other mechanism.

The above results are in contrast to a previously proposed mechanism [12] which suggested that the way in which the corrosive environment increases crack growth rates is through enhanced dissolution of atoms along active slip bands resulting in facet formation. Additionally, since the fracture planes were determined to be crystallographically irrational, and contained significant evidence of localized plasticity, mechanisms assuming cleavage on, or nearly on, (0001) [10] cannot account for the increased crack growth rates either. The fracture planes of some of the facets in the present study are admittedly close to the well known habit plane between the titanium-hydride interface, $\{10\bar{1}7\}$, which, as mentioned earlier, makes it tempting to

relate these observations to the presence of hydrides. Others [9;20] have argued in favor of a hydride formation and fracture mechanism. However, based on the high resolution fractography results obtained in this study (Figure 6 and Figure 7), we find no evidence for hydride precipitation or fracture. There are, however, certain similarities between the facets formed by fracture in H_2 gas (Figure 1) and during SCC. Most notable are the large and small ridges parallel to the crack propagation direction which indicates highly localized plastic flow on the SCC facets. In Figure 1, the hydrides alone cannot account for all of the features consistent with local flow. The other ductile features on the facet surfaces are consistent with the hydrogen assisted localized plasticity mechanism discussed earlier in which hydrogen atmospheres act to locally reduce flow stress permitting highly constrained plastic flow events [16].

In the present study, the facet surfaces contained significant evidence of highly localized plasticity in the form of ridges formed in the crack growth direction when viewed under very high resolution conditions, but were not related to the intersection of slip bands with the fracture surface. Furthermore, these ridges were formed on otherwise macroscopically flat facets that correlated to irrational {hkil} planes of the crystal lattice. Neglecting the three isolated facets near the crack initiation side of the as-received specimen, the primary commonality among all of the facets analyzed was that they favored spatial orientations more nearly perpendicular to the loading direction than inclined to it. While there was certainly an orientation dependence relying on the orientation of the basal pole with regard to facet formation, the actual plane of fracture appeared to favor mode I loading indicating that a high strain energy release rate was an important factor. The irrational facet plane nearly perpendicular to the loading direction is formed by a collection of successive increments of crack growth. It is proposed that hydrogen rich regions at the crack tip facilitate dislocation glide on rational planes (either the basal slip or pyramidal <c+a> slip, depending on the grain orientation) which flow locally leading to the accumulation of large strains at the crack tip. These regions eventually fail by ductile fracture when the ligament between the upper and lower fracture surface is

formed. This mechanism provides progressive and continual crack growth where the crack tip encounters each new grain in succession. There is no fractographic evidence to suggest that there is secondary crack nucleation ahead of the crack tip and subsequent joining with the primary crack tip.

While the above mechanism can explain how the facets are formed on irrational planes, it cannot explain the significantly shorter time-to-failure of the aged specimen. This point can be considered on several levels of detail, all of which likely contributed to the overall difference in time to failure. First, there were no facets directly bordering the surface of the specimen and so there was an increased incubation time before crack formation and faceted crack propagation. On the other hand, the faceted regions directly bordered the specimen surface in the aged specimen (decreased incubation time), and furtheremore, there was a single faceted region that extended across the entire diameter of the specimen providing an easy crack extension path. Since these bands are related to the elongated microtextured regions in the bar (Figure 3), and crack propagation occurs most rapidly by faceted growth, the difference in the relative area of faceted fracture on each specimen further contributes to the difference in time to failure. Once the faceted regions fractured, the stress intensity imposed on the remaining ligament of the specimen was sufficiently large that ductile fracture occurred easily.

The effect of aging on the slip character of the alloy may also help explain the higher growth rates within the faceted region on the aged specimen on a continuum level. While the facet formation process is believed to be related to a highly localized dislocation phenomenon due to hydrogen interactions, the macroscopic crack still has a plastic-zone that must be accommodated by moving dislocations. Since the presence of Ti_3Al tends to result in slip localization [7], it has the effect of constraining the continuum level plastic zone. This results in a decrease in the degree of crack tip blunting during crack extension. A sharp crack tip has a larger stress concentration than a more blunt one which, in this case, is the driving force for

hydrogen migration to the crack tip, ultimately facilitating further crack extension. Indeed, a similar argument has been proposed previously by Curtis et al. [4] and the present results are consistent with their findings.

Conclusions

In the present study, we have demonstrated that faceted crack propagation during SCC does not occur on rational, low index crystallographic slip planes and thus mechanisms based on slip followed by facet formation along the slip band cannot account for the increased crack growth rates. The crystallographic fracture plane was determined to be inclined between 5^{o} and 15^{o} from the basal plane using the quantitative tilt fractography / EBSD method. In general, it was found that the facet planes were spatially oriented nearly perpendicular to the loading axis implying a mode I dominated crack extension criterion. However, ultra-high resolution fractography provided direct evidence of highly localized plastic flow during facet formation indicating that the fracture mechanism was not conventional cleavage. The experimental observations are most consistent with fracture occurring due to the hydrogen enhanced localized plasticity mechanism whereby plastic flow occurs in the immediate vicinity of the crack tip but is constrained and localized such that there is not significant blunting of the crack tip. This mechanism can adequately explain the SCC phenomenon in titanium alloys without the need to invoke a hydride nucleation, growth and fracture mechanism. The presence of the ordered α_2 phase resulted in significantly shorter time to failure, which was believed to be due to restriction of crack tip blunting caused by slip localization within the continuum level plastic zone, although additional chemical factors cannot be ruled out based on the experiments conducted here.

Acknowledgements

The authors would like to thank Dr. S. Fox (Timet, Henderson, Nevada) for providing the Ti-811 bar stock used in this work. The authors are grateful to the Federal Aviation Administration (Grant 08-G-009) for funding this work. One of the authors (ALP) would also like to acknowledge support from Air Force Contract FA8650-07-D-5800 during the preparation of this manuscript.

References

[1] B.F. Brown, Fundamentals, in: B.F. Brown, (Eds.), Stress Corrosion Cracking in High Strength Steels and in Titanium and Aluminum Alloys, Naval Research Lab, Washington, DC, 1972 pp. 1-16.

[2] G. Lütjering, J.C. Williams, Titanium, Springer, New York, NY, 2003, p. 67.

[3] M.J. Blackburn, W.H. Smyrl, J.A. Feeney, Titanium Alloys, in: B.F. Brown, (Eds.), Stress Corrosion Cracking in High Strength Steels and in Titanium and Aluminum Alloys, Naval Research Lab, Washington, DC 1972 pp. 245-363.

[4] R.E. Curtis, R.R. Boyer, J.C. Williams, Trans. of the ASM. 62 (1969) 457-469.

[5] M.J. Blackburn, J.C. Williams, Metallurgical Aspects of the Stress Corrosion Cracking of Titanium Alloys, in: Proceedings of the Conference on Fundamental Aspects of Stress Corrosion Cracking, The Ohio State University, Columbus, OH, 1967 pp. 620-636.

[6] J.C. Williams, A.W. Sommer, P.P. Tung, The Influence of Oxygen Concentration on the Internal Stress and Dislocation Arrangements in α Titanium, Metallurgical Transactions. 3 (1972) 2979-2984.

[7] J.C. Williams, R.G. Baggerly, N.E. Paton, Deformation Behavior of HCP Ti-Al Alloy Single Crystals, Metallurgical and Materials Transactions A. 33 (2002) 837-850.

[8] D.A. Meyn, An Analysis of Frequency and Amplitude Effects on Corrosion Fatigue Crack Propogation in Ti-8Al-1Mo-1V, Metall. Mater. Trans. A. 2 (1971) 853-865.

[9] J.K. Gregory, H.G. Brokmeier, The relationship between crystallographic texture and salt water cracking susceptibility in Ti-6Al-4V, *Mat. Sci. Eng. A.* 203 (1995) 365-372.

[10] E. Richey, R.P. Gangloff, Strain Rate Dependent Environment Assisted Cracking of alp-Ti Alloys in Chloride Solution, in: R. D. Kane, (Eds.), Environmentally Assisted Cracking: Predictive Methods for Risk Assessment and Evaluation of Materials, Equipment, and Structures, ASTM STP 1401 American Society for Testing and Materials, West Conshohocken, PA, 2000, 105-127.

[11] C.D. Beachem, R.M.N. Pelloux, Electron fractography – a tool for the study of micromechanisms of fracturing processes, in: Fracture toughness testing and its applications, ASTM STP 381, 1965, pp. 210-245.

[12] X.G. Zhang, J. Vereecken, Stress Corrosion Cracking Mechanism of Ti-6Al-4V in Acidic Methanol, Corrosion. 46 (1990) 136-141.

[13] M.S. Yeh, J.H. Huang, Internal hydrogen-induced subcritical crack growth in Ti-6Al-4V, Scripta Mat. 36 (1997) 1415-1421.

[14] M.S. Yeh, J.H. Huang, Hydrogen-induced subcritical crack growth in Ti-6Al-4V alloy, Mat. Sci. Eng. A. 242 (1998) 96-107.

[15] I.M. Robertson, H.K. Birnbaum, Dislocation mobility and hydrogen – a brief review, *in*: Proc. 11th International Conference on Fracture, http://www.icf11.com/proceeding/EXTENDED/5759.pdf, accessed 19 Dec 2009.

[16] D.S. Shih, I.M. Robertson, H.K. Birnbaum, Acta. Metall. 36 (1988) 111.

[17] J.C. Williams, Hydride formation, *in* Effect of Hydrogen on Behavior of Materials, A.W. Thompson and I. M. Bernstein, eds., AIME, NY, 1976, p 367-381.

[18] A.L. Pilchak, R.E.A. Williams, J.C. Williams, Crystallography of fatigue crack initiation and growth in fully lamellar Ti-6Al-4V, Met. Mater. Trans. A. 41A (2010) 106-124.

[19] A.W. Thompson, Fractography and its role in fracture interpretation, Fatigue and Fracture of Engineering Materials and Structures, 19 (1996) p. 1307-1316.

[20] N.R. Moody, J.E. Costa, A Review of Microstructure Effects on Hydrogen-Induced Sustained Load Cracking In Structural Titanium Alloys, in: Y.W. Kim and R.R. Boyer, (Eds.), Microstructure/Property Relationships in Titanium Aluminides and Alloys, The Minerals, Metals and Materials Society, 1991, pp. 587-604.

[21] H.J. Rack, J.W. Munford, Environmental Cracking Behavior of Ti-6Al-6V-2Sn: Influence of Alloy Chemistry, in: M.R. Louthan, Jr., R.P. McNitt, and R.D. Sisson (Eds.), Environmental Degradation of Engineering Materials in Hydrogen, VPI Press, Blacksburg, VA, 1981, pp. 369-381.

[22] R.E. Curtis, R.R. Boyer, J.C. Williams, Relationship Between Composition, Microstructure, and Stress-Corrosion Cracking (in Salt Solution) in Titanium Alloys, Transactions of the ASM. 62 (1969) 457-469.

[23] A.L. Pilchak, PhD Dissertation, The Ohio State University, Department of Materials Science and Engineering, 2009.

[24] A.L. Pilchak, J.C. Williams, Observations on the role of hydrogen in facet formation in near-α titanium, under consideration, Met. Mater. Trans. A. (manuscript available upon request).

[25] D.A. Meyn, Effect of Hydrogen on Fracture and Inert-Enviornment Sustained Load Cracking Resistance of α-β Titanium Alloys, *Metall. Trans. A. 5* (1974) 2405-2414.

[26] N.E. Paton, R.A. Spurling, Hydride habit planes in titanium-aluminum alloys, Met. Mater. Trans. A. 7A (1976) 1769-1774.

[27] D.C. Slavik, J.A. Wert, R.P. Gangloff, Determining fracture facet crystallography using backscatter patterns and quantitative tilt fractography, Journal of Materials Research. 8 (1993) 2482-2491.

[28] V. Sinha, M.J. Mills, J.C. Williams, Crystallography of Fracture Facets in a Near-Alpha Titanium Alloy, Metallurgical and Materials Transactions A. 37 (2006) 2015-2026.

[29] V. Sinha, M.J. Mills, J.C. William, Determination of crystallographic orientation of dwell-fatigue facture facets in Ti-6242 alloy, Journal of Materials Science. 42 (2007) 8334-8341.

[30] Y.J. Ro, S.R. Agnew, R.P. Gangloff, Uncertainty in the determination of fatigue facet crystallography, Scripta Materialia. 52 (2005) 531-536.

[31] V. Sinha, J.W. Spowart, M.J. Mills, J.C. Williams, Observations on the Faceted Initiation Site in the Dwell-Fatigue Tested Ti-6242 Alloy: Crystallographic Orientation and Size Effects, Metallurgical and Materials Transactions A. 37 (2006) 1507-1518.

[32] T.R. Bieler, S.L. Semiatin, The origins of heterogeneous deformation during primary hot working of Ti-6Al-4V, International Journal of Plasticity. 18 (2002) 1165-1189.

[33] R.H. Van Stone, J.R. Low, Jr. and J.L. Shannon Jr.: Investigation of the Fracture Mechanism of Ti-5Al-2.5Sn at Cryogenic Temperatures, Metallurgical Transactions A, 9 (1978) p. 539-547.

[34] A.L. Pilchak, J.C. Williams, Crystallography of fluted fracture in near-α titanium alloys, Metall. Mater. Trans. A. 41 (2010) 22-25.

[35] J.C. Chesnutt, J.C. Williams, Comments on the electron fractography of α-titanium, Metall. Mater. Trans. A. 8 (1972) 514-515.

[36] J.C. Chesnutt, C.G. Rhodes, J.C. Williams, Relationship Between Mechanical Properties, Microstructure and Fracture Topography in α + β Titanium Alloys, American Society for Testing and Materials, Fractography-Microscopic Cracking Processes, ASTM STP 600. (1976) 99-138.

[37] A.L. Pilchak, A. Bhattacharjee, A.H. Rosenberger, J.C. Williams, Low ΔK faceted crack growth in titanium alloys, International Journal of Fatigue. 31 (2009) 989-994.

[38] V. Hasija, S. Ghosh, M.J. Mills, D.S. Joseph, Deformation and creep modeling in polycrystalline Ti-6Al alloys, Acta Materialia. 51 (2003) 4533-4549.

[39] S. Suresh, Fatigue of Materials, second ed., Cambridge University Press, New York, 1998.

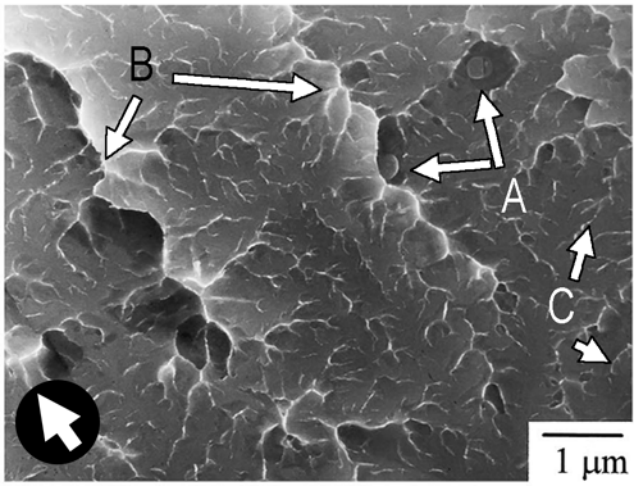

Figure 1. Reproduction of Figure 7 from [14] showing (A) fractured hydrides on a facet surface, (B) primary tear ridges and (C) smaller, secondary tear ridges. The encircled arrow denotes the local crack propagation direction.

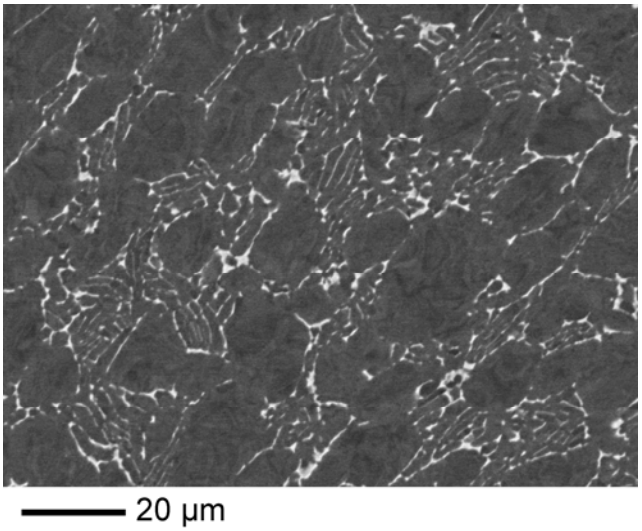

Figure 2. Microstructure of the as-received mateiral transverse to the bar axis.

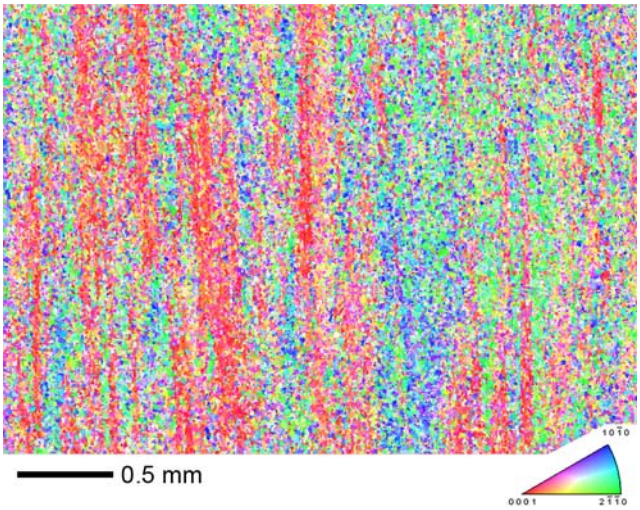

Figure 3. Inverse pole figure map of the Ti-811 bar material. The tensile axis of the specimens is perpendicular to the plane of the image. The {hkil} plane parallel to the plane of the image in each region is identified by the color coded unit triangle.

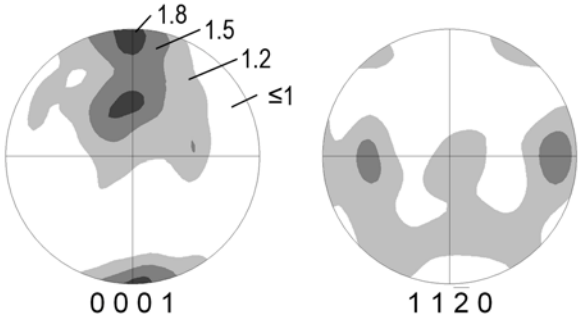

Figure 4. Equal angle projections showing the texture of the as-received bar. The tensile axis of the specimens is perpendicular to the plan of the projection.

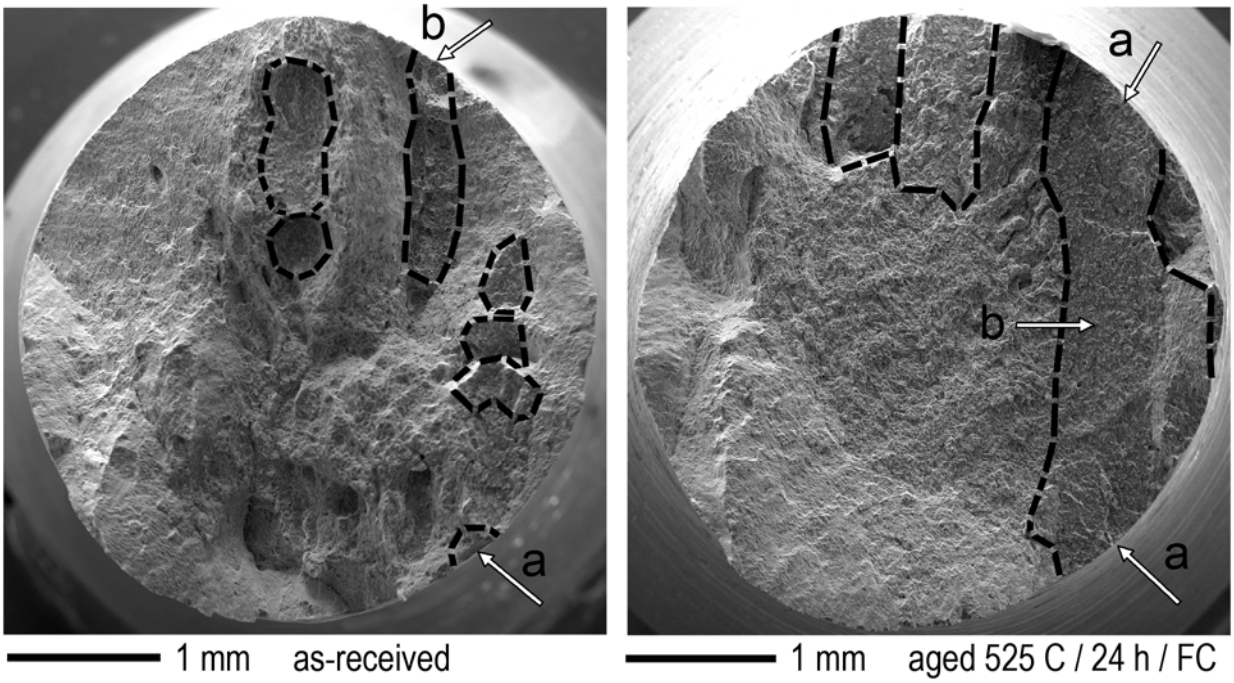

Figure 5. Low magnification secondary electron images of the cross sections of the fractured specimens. The regions corresponding to faceted fracture topography are enclosed by the black dashed lines. The sites identified by ‘a’ and ‘b’ correspond with sites that are characterized as initiation and propagation facets, respectively.

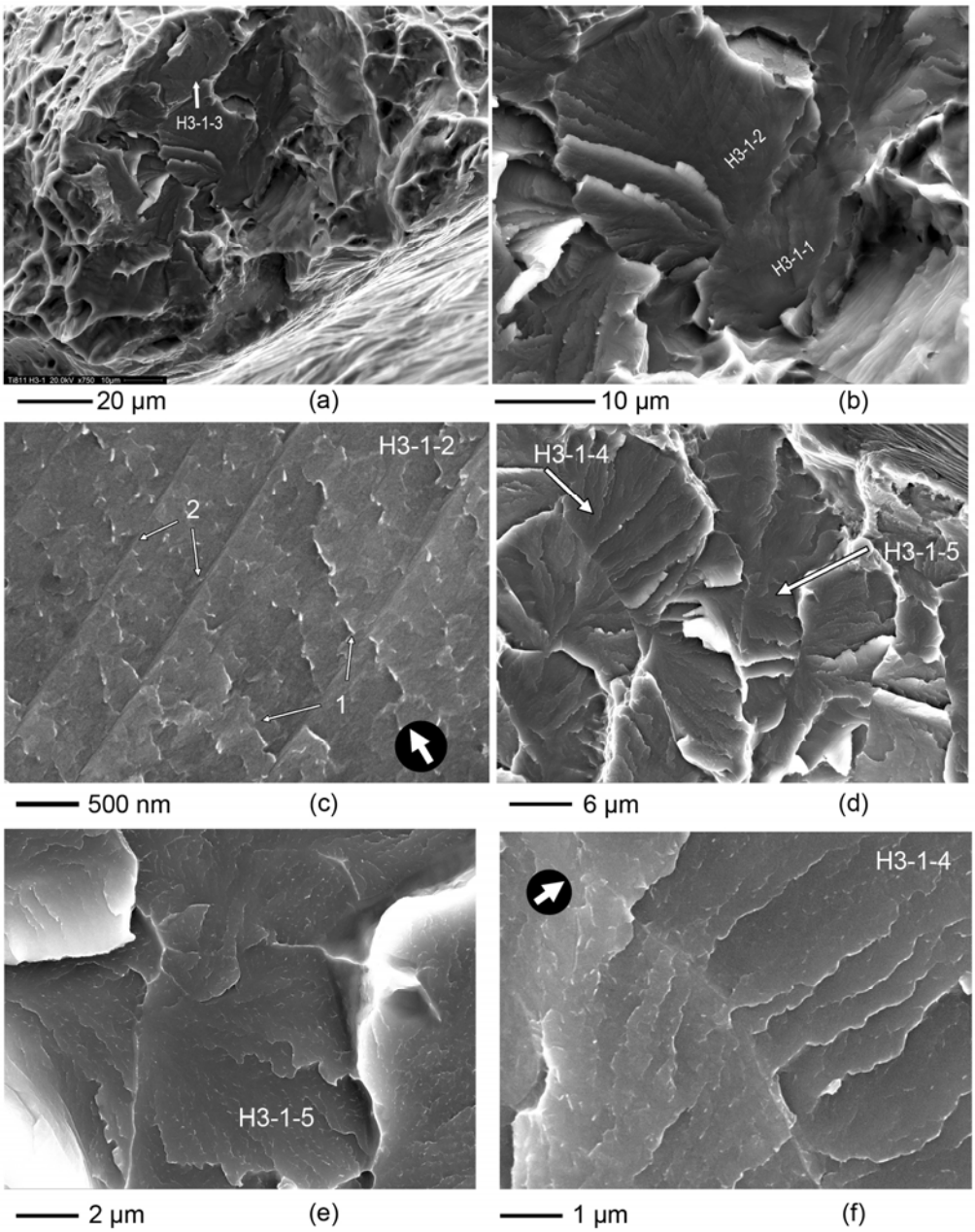

Figure 6. Fractography of the as-received specimen. (a), (b) and (c) correspond to the initiation facets while (d), (e) and (f) are images of propagation facets. In (c), the encircled arrow designates the direction of crack propagation.

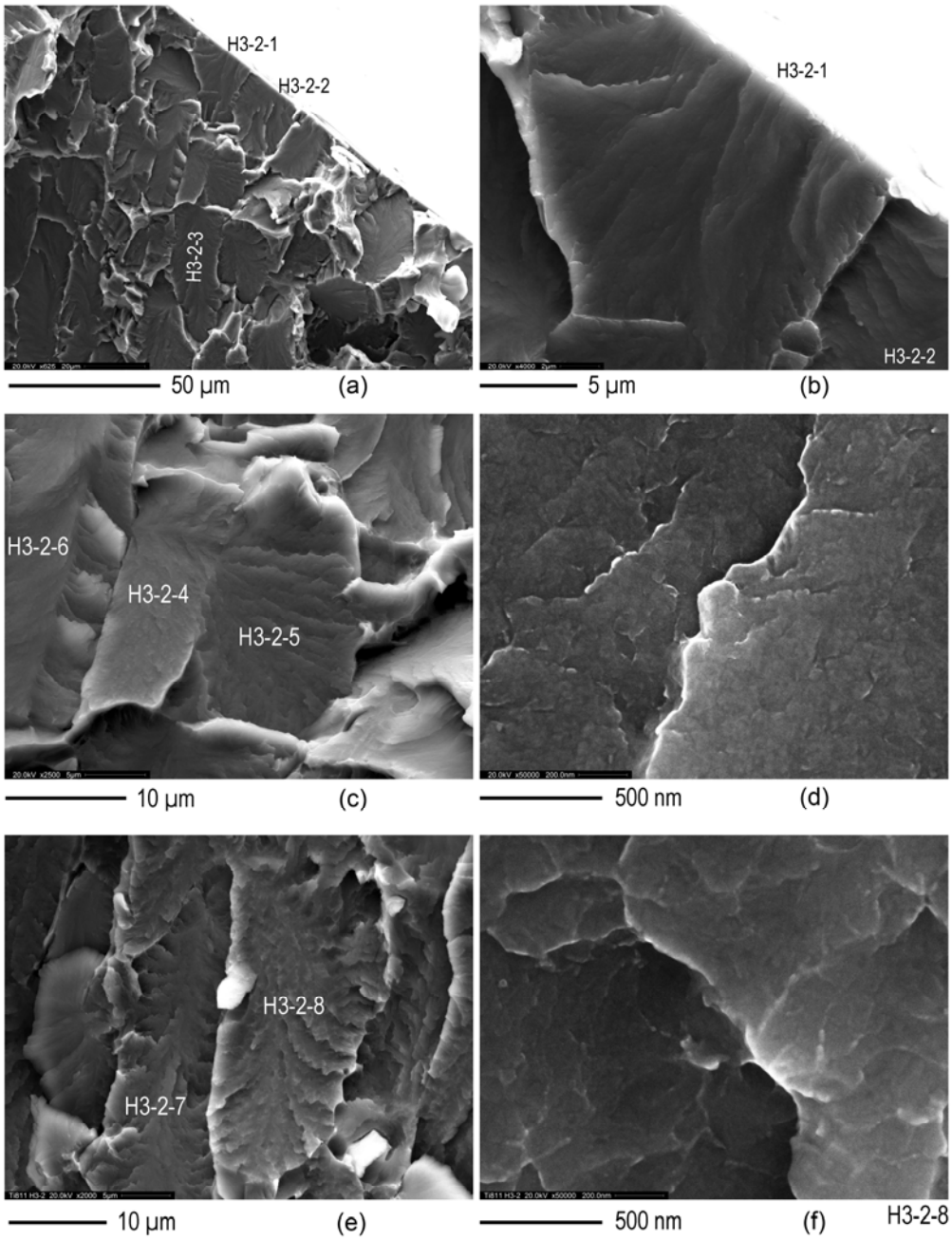

Figure 7. Fractography of the aged specimen. Facets H3-2-7 and H3-2-8 in (e) and (f) were observed at a crack length of ~1 mm.

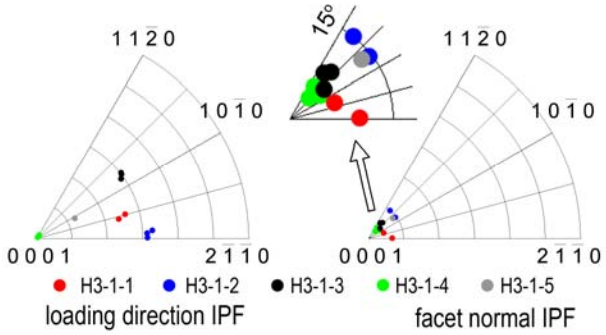

Figure 8. Facet crystallography of the as-received specimen (H3-1).

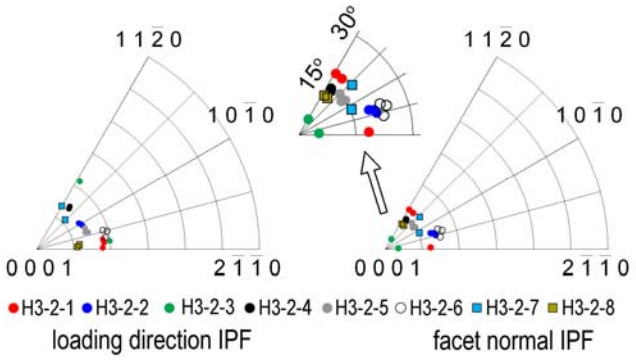

Figure 9. Facet crystallography for the aged SCC specimen (H3-2).

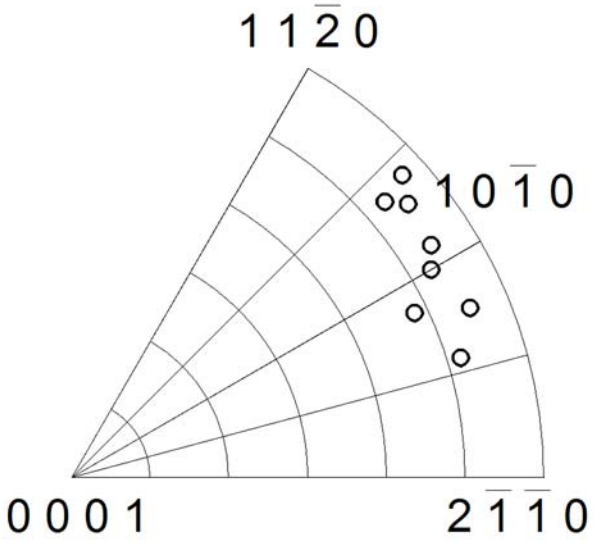

Figure 10. In-plane crack propagation direction orientation measurements. Each point on the equal angle projection represents the orientation of grain H3-1-4 with respect to unit vectors parallel to one of the ridges on the facet surfaces.

Tables and table captions:

Table 1. Quantitative tilt fractography results for the as-received specimen (H3-1). The angles between the loading direction (LD) and facet normal (n), the facet normal and the [0001] direction and the [0001] direction and the LD are reported in degrees.

Facet ID	n / LD	n / [0001]	[0001] / LD	facet normal vector
1	29.1	7.6	36.5	+0.4850i +0.0351j +0.8738k
2	36.3	14.0	46.8	+0.5814i +0.1077j +0.8064k
3	37.0	7.1	44.6	+0.5261i +0.2917j +0.7988k
4	6.8	5.5	0.8	-0.0235i +0.1166j +0.9929k
5	8.3	10.9	17.5	-0.0118i +0.1444j +0.9894k

Table 2. Quantitative tilt fractography results for the aged specimen (H3-2). The angles between the loading direction (LD) and facet normal (n), the facet normal and the [0001] direction and the [0001] direction and the LD are reported in degrees.

Facet ID	n / LD	n / [0001]	[0001] / LD	facet normal vector
1	8.9	17.7	26.2	-0.1541i -0.0090j +0.9880k
2	4.3	19.6	19.4	-0.0509i +0.0546j +0.9972k
3	27.1	4.5	30.3	-0.4318i +0.1457j +0.8901k
4	7.0	13.6	20.6	+0.1067i +0.0567j +0.9927k
5	8.7	13.6	20.6	-0.1481i +0.0270j +0.9886k
6	5.6	22.3	27.6	-0.0171i +0.0958j +0.9952k
7	7.1	10.0	17.0	+0.1156i + 0.0431j + 0.9924k
8	7.2	11.3	16.1	+0.1171i + 0.0460j + 0.9920k